J. Phys.: Condens. Matter **21** (2009) 344206 (5pp) doi:10.1088/0953-8984/21/34/344206

On spectral properties of bilayer graphene: the effect of an SiC substrate and infrared magneto-spectroscopy

M Mucha-Kruczyński[1], D S L Abergel[1,2], E McCann[1] and V I Fal'ko[1]

[1] Department of Physics, Lancaster University, Lancaster LA1 4YB, UK
[2] Department of Physics and Astronomy, University of Manitoba, Winnipeg, R3T 2N2, Canada

E-mail: m.mucha-kruczynski@lancaster.ac.uk

Received 23 October 2008, in final form 27 October 2008
Published 27 July 2009
Online at stacks.iop.org/JPhysCM/21/344206

Abstract
We investigate the effect of asymmetry in bilayer graphene induced by a diatomic substrate (such as SiC) and its influence on the bilayer spectrum in zero and strong magnetic fields. We also determine selection rules for inter-Landau level transitions, taking into account all four π bands.

The discovery of self-standing graphene—planes of carbon atoms arranged in a honeycomb lattice [1]—stimulated intense studies of monolayer and bilayer graphene structures (see [2–5] for reviews). In particular, interest in the development of epitaxial growth techniques for graphene attracted attention to the possibility of synthesizing graphite films by sublimation of Si from SiC [6–8], where the substrate induces symmetry breaking in the overlying graphene sheet, which is especially pronounced in monolayer and bilayer materials. Also, interest in optical properties of graphene resulted in several experimental magneto-optics studies of graphene in FIR, IR and the visible range [9–14].

In this paper, we investigate the combined effect of intralayer and interlayer asymmetries caused by a substrate on the electronic spectra of bilayer graphene, both with and without applied magnetic field. We show that intralayer asymmetry leads to the opening of an indirect gap with a 'Mexican hat'-type feature in one of the bands (whether conduction or valence depends on the sign of the asymmetry) and to an asymmetric density of states (DOS). This is different to the DOS in 'biased' bilayer graphene [15–19], where the gap is the result of broken symmetry between the layers (realized experimentally in [16, 20, 21]). In external magnetic field, both asymmetries lift the valley degeneracy and split the low-energy $n = 0$ and 1 Landau levels (LLs). Finally, we determine the optical strengths of inter-LL transitions.

A schematic view of bilayer graphene (marked with the hopping integrals considered throughout this paper) and the Brillouin zone of bilayer graphene are shown in figure 1(a). Bilayer graphene consists of two coupled hexagonal lattices with inequivalent sites A1, B1 and A2, B2 in the first and second graphene sheets, respectively, which are arranged according to Bernal (A2–B1) stacking [22]. The hexagonal Brillouin zone has two inequivalent degeneracy points with wavevectors $\mathbf{K}_\xi = (\xi\frac{4\pi}{3a}, 0)$ (where $\xi \in \{+,-\}$ and a is the lattice constant). We restrict ourselves to nearest neighbour in-plane and A1(2) $\leftrightarrow$ B2(1) interactions in the tight-binding approximation of π orbitals $\psi_{\mu i}(\mu \in \{\mathrm{A},\mathrm{B}\}, i \in \{1,2\})$ and parametrize hopping integrals and on-site asymmetries according to the Slonczewski–Weiss–McClure model [23, 24]. After expansion of the momentum $\mathbf{p}$ around the K points: $\mathbf{p} = \hbar\mathbf{K}_\xi + \mathbf{q}$, we write the Hamiltonian in the basis $\Psi_+ = (\psi_{\mathrm{A1}}, \psi_{\mathrm{B2}}, \psi_{\mathrm{A2}}, \psi_{\mathrm{B1}})^{\mathrm{T}}$ in the valley K_+ and $\Psi_- = (\psi_{\mathrm{B2}}, \psi_{\mathrm{A1}}, \psi_{\mathrm{B1}}, \psi_{\mathrm{A2}})^{\mathrm{T}}$ in K_- [22]:

$$\hat{H} = \xi \begin{pmatrix} \frac{U}{2} + \frac{\Delta}{4}(1+\xi) & v_3\pi & 0 & v\pi^\dagger \\ v_3\pi^\dagger & -\frac{U}{2} - \frac{\Delta}{4}(1-\xi) & v\pi & 0 \\ 0 & v\pi^\dagger & -\frac{U}{2} + \frac{\Delta}{4}(1-\xi) & \xi\gamma_1 \\ v\pi & 0 & \xi\gamma_1 & \frac{U}{2} - \frac{\Delta}{4}(1+\xi) \end{pmatrix}; \quad (1)$$

where $v = \frac{a\sqrt{3}}{2\hbar}\gamma_0$, $v_3 = -\frac{a\sqrt{3}}{2\hbar}\gamma_3$ and $\pi = q_x + \mathrm{i}q_y$. The parameter U describes an energy difference between sites on different layers (interlayer asymmetry), whereas Δ is the

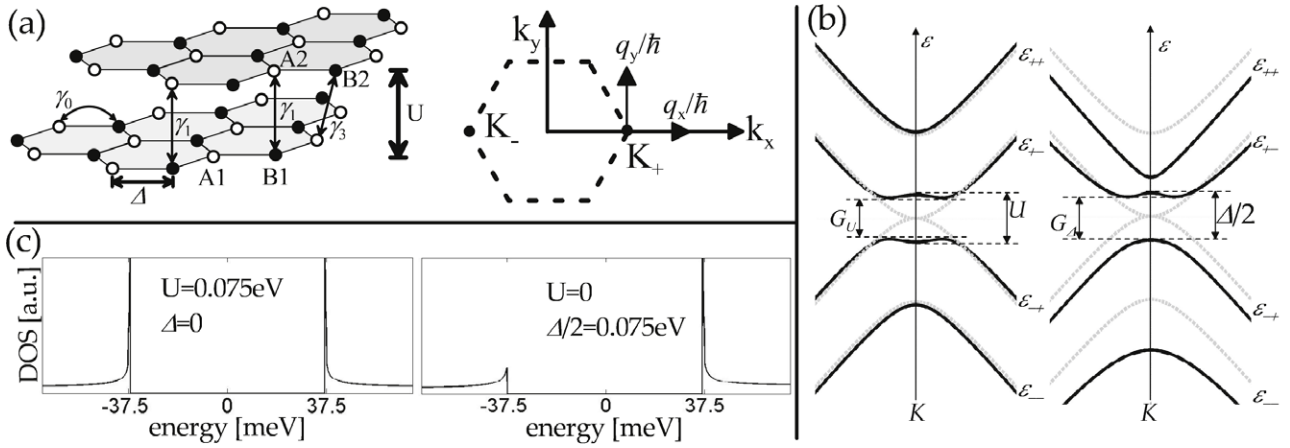

Figure 1. (a) On the left: schematic view of the bilayer graphene lattice containing four atoms in the unit cell: A1 (white circles) and B1 (black) in the bottom layer and A2 (white) and B2 (black) in the top one; also shown are the hopping parameters used in the tight-binding model and on-site energy asymmetries. On the right: first Brillouin zone of bilayer graphene. (b) On the left (right): cross-section of the band structure around the K point in the conical approximation in the presence of interlayer (intralayer) on-site asymmetry U (Δ); grey lines show the band structure with no on-site asymmetry (U, $\Delta = 0$); on both graphs, the middle of the gap at the K point is chosen as the zero of the energy scale. (c) In the left (right) graph: DOS in the vicinity of the gap $G \approx 75$ meV opened by interlayer (intralayer) asymmetry $U = 75$ meV ($\Delta/2 = 75$ meV). DOS was evaluated using the effective low-energy model [22]. Values of parameters used in (b) and (c): $\gamma_0 = 3.0$ eV, $\gamma_1 = -0.35$ eV, $a = 2.46$ Å, resulting in low-energy effective mass $m_{\text{eff}} = |\gamma_1|/2v^2 \approx 0.03$ of the electron mass.

asymmetry between sites A1 and B1 in the bottom layer due to the underlying substrate (intralayer asymmetry). Having neglected a small v_3-term, we arrive at the electron spectrum for a symmetric bilayer ($U = 0$, $\Delta = 0$) shown with grey lines in figure 1(b) and given by:

$$\epsilon_{\alpha\beta} = \alpha \tfrac{1}{2}\left(\sqrt{\gamma_1^2 + 4v^2q^2} + \beta\gamma_1\right), \qquad (2)$$

where α and β are $+$ or $-$ and $q = \sqrt{q_x^2 + q_y^2}$ is the magnitude of momentum measured from the K point. On the other hand, black lines in figure 1(b) present the typical structure of the π bands close to the K point for each kind of on-site asymmetry separately. Interlayer asymmetry ($U \neq 0, \Delta = 0$), left side of figure 1(b), leads to the opening of a gap such that the conduction and valence bands are symmetric with respect to the middle of the gap. Low-energy bands (ϵ_{+-} and ϵ_{-+}) are pushed upwards at the K point leading to a 'Mexican hat' structure with increasing U [15, 18, 19]. In this case, the direct band gap is $G_U = \frac{|\gamma_1 U|}{\sqrt{\gamma_1^2+U^2}}$. High-energy bands, ϵ_{++} and ϵ_{--}, are shifted away from the neutrality point (that is, the point where the low-energy bands touch at the K point for $U, \Delta = 0$) without a significant change in shape. In the case of intralayer asymmetry ($U = 0, \Delta \neq 0$), right side of figure 1(b), a gap opens such that the conduction and valence bands are asymmetric with respect to the middle of the gap at the K point at energy $\epsilon = \frac{|\Delta|}{4}$. The asymmetry depends on the sign of Δ and here we shall discuss the case when $\Delta > 0$ (switching the sign of Δ leads to a mirror reflection of the band structure with respect to the middle of the gap). The low-energy bands split: the ϵ_{-+} band shifts downwards with little change in shape while the band ϵ_{+-} is strongly pushed upwards at the K point giving rise to a 'Mexican hat' structure at the bottom of the conduction band. At the same time, both high-energy bands remain parabolic and are shifted downwards with increasing Δ. This results in an indirect gap in the electronic spectrum $G_\Delta = \frac{|\Delta|}{4}(1 + \sqrt{1 - \frac{\Delta^2}{4\gamma_1^2}})$ and the possibility, for very strong asymmetry $\Delta = \gamma_1\sqrt{2}$, of bands ϵ_{++} and ϵ_{+-} touching at the K point. Increasing Δ further leads to a shift of the high-energy parabolic band upwards and the low-energy one downwards. For $\Delta^{\text{M}} = \gamma_1\sqrt{3}$, the band gap G_Δ reaches a maximum value $G_\Delta^{\text{M}} = \frac{3\sqrt{3}\gamma_1}{8}$. This value is smaller than the maximum interlayer asymmetry gap $G_U^{\text{M}} = |\gamma_1|$. Also, for strong asymmetry the 'Mexican hat' feature is destroyed and, for $\Delta > \Delta^{\text{M}}$, the gap actually decreases with $\lim_{\Delta\to\infty} G_\Delta = 0$. For a given small value of asymmetry, Δ opens a gap approximately half as big as that due to U. All comparisons between the effects of Δ and U in this paper are made for the same value of the gap at the K point, thus using the same numerical values for $\Delta/2$ and U.

We point out that two characteristic features allow for distinguishing between inter and intralayer asymmetry induced by the substrate in the system. In particular, in the case of intralayer asymmetry, the 'Mexican hat' is present only in one low-energy band (whether valence or conduction depends on the sign of Δ [25]). Although its size in momentum space is small, it causes significant changes in the DOS at the top of the valence and bottom of the conduction bands as shown in figure 1(c). In all cases, spikes indicate where the Mexican hat is present, and the step behind each spike corresponds to the top of the hat and the cross over to almost parabolic bands. Also, if the sublattice symmetry is broken, the position of the high-energy bands with respect to the low-energy ones is strongly asymmetric.

In the presence of magnetic field B perpendicular to the graphene sheet, the Landau level (LL) spectrum forms. This spectrum can be obtained for the Hamiltonian in equation (1) by using the Landau gauge $\mathbf{A} = (0, -Bx)$ and the fact that

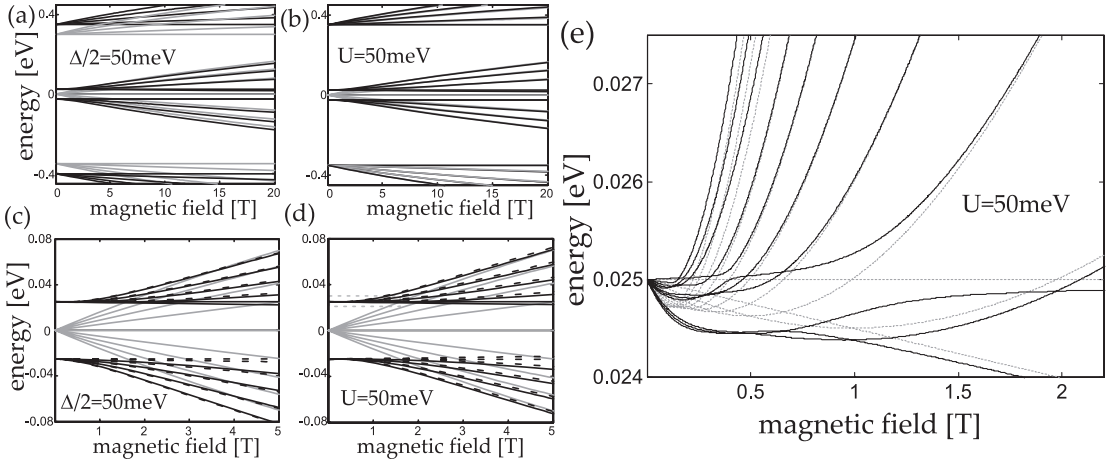

Figure 2. Numerically computed Landau levels of bilayer graphene ($n = 0, 1, 2, 3, 4$) for range of high ((a) and (b)) and low ((c) and (d)) energies; black solid and dashed lines in (c) and (d) represent levels at valley K_+ and K_- respectively, grey solid lines in the background show the Landau level spectrum for no asymmetries ($U, \Delta = 0$); in (a) and (b) only the spectrum at K_+ is shown for clarity. Note that nonzero U in (b) affects the high-energy LLs very weakly and so the corresponding grey lines are underneath the black ones. Zero of the energy scale is shifted to the middle of the gap opened in each case at the K point. (e) Area bounded by dashed grey rectangle in (d) shown again with the 11 lowest LLs at K_+: black solid lines—taking into account $\gamma_3 = -0.15$ eV; grey dashed lines— γ_3 neglected. The interlevel crossings are a signature of the Mexican hat structure present in the electronic spectrum of this band. Inclusion of v_3 leads to a separation of the LLs into groups of three with interlevel crossings among levels in the same branch but anticrossings between levels in different branches. Values of parameters used: $v = 1 \times 10^6$ m s^{-1}, $\gamma_1 = -0.35$ eV, resulting in low-energy effective mass $m_{\text{eff}} = |\gamma_1|/2v^2 \approx 0.03$ of the electron mass.

operators $\pi = q_x + \mathrm{i}q_y + e(A_x + \mathrm{i}A_y)$ and $\pi^\dagger = q_x - \mathrm{i}q_y + e(A_x - \mathrm{i}A_y)$ are the same as lowering (raising) operators in the basis of Landau functions $\psi_n(x, y) = \mathrm{e}^{\mathrm{i}q_y y/\hbar}\phi_n(x + q_y\lambda_B^2)$ (where $\phi_n(x)$ are the wavefunctions of a quantum harmonic oscillator),

$$\pi\psi_n = -\mathrm{i}\frac{\hbar}{\lambda_B}\sqrt{2n}\psi_{n-1} \qquad \text{and} \qquad \pi\psi_0 = 0; \\ \pi^\dagger\psi_n = \mathrm{i}\frac{\hbar}{\lambda_B}\sqrt{2(n+1)}\psi_{n+1}; \tag{3}$$

where the magnetic length $\lambda_B = \sqrt{\hbar/eB}$. If we neglect v_3, Hamiltonian (1) can be then diagonalized separately for each n [26–28]. In the following, we use superscript c (s) to denote Landau levels originating from low-energy (high-energy) bands and β equal to 1 or -1 to indicate the sign of the energy. Then, in the case of symmetric bilayers ($U, \Delta = 0$), the energy $\epsilon^c_{n\beta}$ of the nth Landau level is given by:

$$\epsilon^c_0 = 0; \qquad \epsilon^c_1 = 0; \tag{4a}$$

$$\epsilon^c_{n\beta} = \frac{\beta}{\sqrt{2}}\left(\gamma_1^2 + 2\frac{\hbar^2v^2}{\lambda_B^2}(2n-1) - \sqrt{\gamma_1^4 + \frac{4\hbar^2v^2\gamma_1^2}{\lambda_B^2}(2n-1) + \frac{4\hbar^4v^4}{\lambda_B^4}}\right)^{\frac{1}{2}} \qquad \text{for } n \geqslant 2; \tag{4b}$$

and in high-energy bands:

$$\epsilon^s_{n\beta} = \frac{\beta}{\sqrt{2}}\left(\gamma_1^2 + 2\frac{\hbar^2v^2}{\lambda_B^2}(2n-1) + \sqrt{\gamma_1^4 + \frac{4\hbar^2v^2\gamma_1^2}{\lambda_B^2}(2n-1) + \frac{4\hbar^4v^4}{\lambda_B^4}}\right)^{\frac{1}{2}} \qquad \text{for } n \geqslant 1. \tag{5}$$

In this formulation, for high-energy LLs indexing starts with $n = 1$, not 0, emphasizing the distinctiveness of LL $n = 0$. Each level has additional four-fold degeneracy due to valleys and spins. The low-energy Landau level spectrum resulting from equations (4) is shown as grey solid lines in the background in figures 2(c) and (d). Those levels create a fan-plot originating at zero energy. Interestingly, the levels $n = 0$ and 1 have the same energy, leading to an unusual eight-fold degenerate level at zero energy [22, 30]. The high-energy LLs create two additional fan-plots originating at $\epsilon = \pm\gamma_1$ which are shown together with low-energy LLs with grey solid lines in figures 2(a) and (b).

For magnetic fields $B < 20$ T, expressions for the LL energy in a symmetric bilayer, equations (4) and (5), can be simplified using a small parameter $x = \frac{\sqrt{2}\hbar v}{\lambda_B\gamma_1}$; $|x| \ll 1$. Additionally, assuming that U and Δ are small, we obtain energies:

$$\epsilon^c_0 = \xi\left[\frac{U}{2} + \frac{\Delta}{4}(\xi+1)\right]; \tag{6a}$$

$$\epsilon^c_1 \approx \epsilon^c_0 - \xi x^2\left(U + \xi\frac{\Delta}{2}\right); \tag{6a}$$

$$\epsilon^c_{n\beta} \approx \Sigma + \beta\sqrt{\epsilon_n^2 + \Omega^2}, \qquad n \geqslant 2; \tag{6b}$$

$$\epsilon^s_{n\beta} \approx \beta|\gamma_1|\left(1 + x^2\left(n - \frac{1}{2}\right)\right) + \frac{1}{2}\left[\xi U x^2 - \frac{\Delta}{2}\left(1 - x^2(2n-1)\right)\right], \qquad n \geqslant 1; \tag{6c}$$

$$\Sigma = \frac{\Delta}{4} - \frac{\xi x^2}{2}\left[U(2n+1) + \frac{\Delta}{2}(2n-1)(2\xi+1)\right]; \tag{6d}$$

$$\Omega = \frac{\xi}{2}\left(U + \frac{\Delta}{2}\right) - \frac{x^2}{2}\left[\xi U(2n-1) + \frac{\Delta}{4}(2n+1)\right]; \quad (6e)$$

$\epsilon_n = |\gamma_1| x^2 \sqrt{n(n-1)}$.

The numerically calculated Landau level spectra in the presence of asymmetry U and $\Delta/2$ are shown in figures 2(a)–(d) with black solid lines. Due to the asymmetry, valley degeneracy is lifted. Also, the additional degeneracy of $n = 0$ and 1 LLs is removed, $\epsilon_1 \neq \epsilon_0$ (note that even the $n = 0$ level is shifted with respect to the middle of the gap at the K point from $\epsilon = 0$ in opposite directions in the valley $K_+(\xi = +)$ and $K_-(\xi = -)$). As can be seen in figure 2(a), interlayer asymmetry U affects the high-energy LLs very weakly and so corresponding black lines cover grey lines showing high-energy LLs in the symmetric bilayer. At low energies and low fields, signatures of a Mexican hat developing in the electronic spectrum of an asymmetric bilayer can be noticed in the fan-plots of the LL spectrum. Inverted curvature in the central part of such a structure (hole-like in conduction and electron-like in valence band) results in inverted behaviour of Landau levels at very low B (the energy of electron (hole) levels decrease (increase) with increasing B) which then returns to typical behaviour at higher B (the energy of electron (hole) levels increase (decrease) with increasing B). This results in interlevel crossings. Also, this is a regime where the influence of the parameter v_3, neglected so far, is important, because it mixes LLs n and $n-3$ thus changing some of the interlevel crossings into anticrossings. An example of the numerically calculated spectrum taking into account v_3 is shown in figure 2(e).

The wavefunctions corresponding to LLs described in equations (6) are as follows:

$$|\psi_0^c\rangle = \begin{pmatrix} -\mathrm{i}\xi\psi_0 \\ 0 \\ 0 \\ 0 \end{pmatrix}; \quad (7a)$$

$$|\psi_1^c\rangle \approx \begin{pmatrix} -\mathrm{i}\xi\left(1 - \frac{x^2}{2}\right)\psi_1 \\ 0 \\ x\psi_0 \\ 0 \end{pmatrix};$$

$$|\psi_{n\beta}^c\rangle \approx \frac{1}{2\sqrt{\Gamma_n(\Gamma_n + \epsilon_n)}} \times \begin{pmatrix} -\mathrm{i}\xi\left[1 - x^2\left(n - \frac{1}{4}\right)\right](\Gamma_n + \epsilon_n + \beta\Omega)\Psi_n \\ -\mathrm{i}\xi\beta\left(1 + \frac{x^2}{4}\right)(\Gamma_n + \epsilon_n - \beta\Omega)\Psi_{n-2} \\ x\sqrt{n}(\Gamma_n + \epsilon_n + \beta\Omega)\Psi_{n-1} \\ -\beta x\sqrt{n-1}(\Gamma_n + \epsilon_n - \beta\Omega)\psi_{n-1} \end{pmatrix}, \quad n \geqslant 2; \quad (7b)$$

$$|\psi_{n\beta}^s\rangle \approx \frac{1}{\sqrt{2}} \begin{pmatrix} \mathrm{i}\xi x\sqrt{n}\Psi_n \\ -\mathrm{i}\xi\beta x\sqrt{n-1}\Psi_{n-2} \\ \left(1 - \frac{nx^2}{2}\right)\Psi_{n-1} \\ \beta[1 - \frac{x^2}{2}(n-1)]\Psi_{n-1} \end{pmatrix}, \quad n \geqslant 1; \quad (7c)$$

where:

$$\beta = \pm 1; \qquad \Gamma_n = \sqrt{\epsilon_n^2 + \Omega_n^2}. \quad (8)$$

These wavefunctions determine transition rules for the absorption of right ($\oplus$) and left-handed ($\ominus$) circularly polarized light $\mathbf{E}_\omega = E_\omega \mathbf{l}_{\oplus/\ominus}$, with $\mathbf{l}_\oplus = (\mathbf{l}_x - \mathrm{i}\mathbf{l}_y)/\sqrt{2}$ and $\mathbf{l}_\ominus = (\mathbf{l}_x + \mathrm{i}\mathbf{l}_y)/\sqrt{2}$. Using current operator $\mathbf{j} = e(\frac{\partial H}{\partial q_x}, \frac{\partial H}{\partial q_y})$, we find optical strengths of inter-LL transitions (approximated with the first meaningful term in $1/\gamma_1$):

$$|\langle\psi_1^c|\mathbf{j}\cdot\mathbf{l}_\oplus|\psi_0^c\rangle\|^2 = |\langle\psi_0^c|\mathbf{j}\cdot\mathbf{l}_\ominus|\psi_1^c\rangle|^2 \approx \frac{e^2v^2x^2(2\xi U + \Delta)^2}{2\gamma_1^2}; \quad (9a)$$

$$|\langle\psi_{2\beta}^c|\mathbf{j}\cdot\mathbf{l}_\oplus|\psi_1^c\rangle\|^2 \approx 2e^2v^2x^2\Lambda_{2\beta}^{(-)}; \quad (9b)$$

$$|\langle\psi_1^c|\mathbf{j}\cdot\mathbf{l}_\ominus|\psi_{2\alpha}^c\rangle\|^2 \approx 2e^2v^2x^2\Lambda_{2\alpha}^{(-)};$$

$$|\langle\psi_{n\beta}^c|\mathbf{j}\cdot\mathbf{l}_\oplus|\psi_{m\alpha}^c\rangle|^2 \approx e^2v^2x^2m\delta_{n-1,m} \times \frac{\Lambda_{m\alpha}^{(+)}\Lambda_{n\beta}^{(-)}}{2}, \qquad m \geqslant 2; \quad (9c)$$

$$|\langle\psi_{n\beta}^c|\mathbf{j}\cdot\mathbf{l}_\ominus|\psi_{m\alpha}^c\rangle|^2 \approx e^2v^2x^2(m-1) \times \delta_{n,m-1}\frac{\Lambda_{m\alpha}^{(-)}\Lambda_{n\beta}^{(+)}}{2}, \qquad m \geqslant 3; \quad (9d)$$

$$|\langle\psi_{n\beta}^s|\mathbf{j}\cdot\mathbf{l}_\oplus|\psi_m^c\rangle|^2 \approx e^2v^2\delta_{n-1,m}, \qquad m = 0, 1;$$

$$|\langle\psi_{n\beta}^s|\mathbf{j}\cdot\mathbf{l}_\oplus|\psi_{m\alpha}^c\rangle|^2 \approx \frac{e^2v^2\Lambda_{m\alpha}^{(+)}}{4}\delta_{n-1,m}, \qquad m \geqslant 2; \quad (9e)$$

$$|\langle\psi_{n\beta}^s|\mathbf{j}\cdot\mathbf{l}_\ominus|\psi_{m\alpha}^c\rangle|^2 \approx \frac{e^2v^2\Lambda_{m\alpha}^{(-)}}{4}\delta_{n,m-1}, \qquad m \geqslant 2; \quad (9f)$$

$$|\langle\psi_{n\beta}^c|\mathbf{j}\cdot\mathbf{l}_\oplus|\psi_{m\alpha}^s\rangle|^2 \approx \frac{e^2v^2\Lambda_{n\beta}^{(-)}}{4}\delta_{n-1,m}, \qquad m \geqslant 1; \quad (9g)$$

$$|\langle\psi_n^c|\mathbf{j}\cdot\mathbf{l}_\ominus|\psi_{m\alpha}^s\rangle|^2 \approx e^2v^2\delta_{n,m+1}, \qquad m = 1, 2;$$

$$|\langle\psi_{n\beta}^c|\mathbf{j}\cdot\mathbf{l}_\ominus|\psi_{m\alpha}^s\rangle|^2 \approx \frac{e^2v^2\Lambda_{n\beta}^{(+)}}{4}\delta_{n,m-1}, \qquad m \geqslant 3; \quad (9h)$$

$$|\langle\psi_{n\beta}^s|\mathbf{j}\cdot\mathbf{l}_\oplus|\psi_{m\alpha}^s\rangle|^2 \approx 2e^2v^2x^2m\delta_{n-1,m}, \qquad m \geqslant 1; \quad (9i)$$

$$|\langle\psi_{n\beta}^s|\mathbf{j}\cdot\mathbf{l}_\ominus|\psi_{m\alpha}^s\rangle|^2 \approx 2e^2v^2x^2(m-1)\delta_{n,m-1}, \qquad m \geqslant 2; \quad (9j)$$

where:

$$\Lambda_{m\alpha}^{(\mu)} = \frac{(\Gamma_m + \epsilon_m + \mu\alpha\Omega)^2}{\Gamma_m(\Gamma_m + \epsilon_m)}; \quad (10)$$

$$\Lambda_{m\alpha}^{(\mu)} = 2 \qquad \text{for } U, \Delta = 0.$$

Equations in (9) generalize the earlier study of optical and magneto-optical absorption in bilayers [29]. Examples of allowed transitions are illustrated in figures 3(a) and (b). Independently of the presence/absence of asymmetries Δ or U, selection rules for absorption of right-handed polarized light are such that the Landau level index has to be decreased by one, whereas absorption of left-handed photons requires an increase of the Landau level index by one. Also, optical strengths of $c \to c$ and $s \to s$ transitions are proportional to the magnetic field B and LL index, whereas optical strengths of $s \leftrightarrow c$ transitions are almost independent of B. As x is a small parameter, the intensity of the first $s \leftrightarrow c$ transitions should be higher than for $c \to c$ transitions corresponding to the same energy of incident radiation $\hbar\omega$. In figure 3(c), the numerically calculated magneto-optical spectrum of symmetric bilayer for

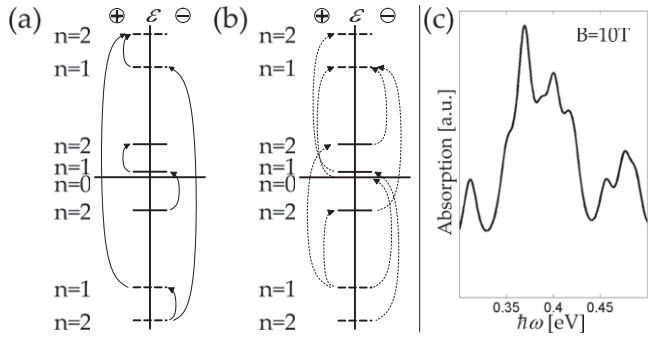

Figure 3. Allowed intraband (a) and interband (b) optical excitations. Low-energy (high-energy) LLs are depicted with solid (dashed) lines. Transitions in $\mathbf{l}_{\oplus}$ ($\mathbf{l}_{\ominus}$) are shown on the left (right) of the energy axis, under $\oplus$ ($\ominus$) symbol. Energy axis not to scale; not shown is very weak $|0_c\rangle \rightarrow |1_c\rangle$ transition allowed only in the presence of asymmetry. (c) Magneto-optical absorption spectrum for the energy of incident light $\hbar\omega \approx |\gamma_1|$; magnetic field $B = 10$ T, $\gamma_1 = -0.35$ eV, $v = 10^6$ m s^{-1}; Landau level broadening was approximated with Lorentzian with full width at half maximum 20 meV.

$\hbar\omega \approx |\gamma_1|$ has been shown with the same broadening of all Landau levels assumed. Indeed, the two highest peaks are due to the first $s \leftrightarrow c$ transitions against the background of $c \rightarrow c$ excitations.

In summary, we have shown how a substrate-induced asymmetry affects the band structure of bilayer graphene grown on SiC. Sublattice-symmetry breaking in the bottom layer results in the opening of an indirect gap with a 'Mexican hat'-type feature in either the conduction or the valence band depending on the sign of the 'symmetry breaking parameter', Δ, whereas interlayer asymmetry leads to the appearance of similar features in both low-energy bands. We have also investigated the influence of the asymmetry gap on the Landau level spectrum. Either of the asymmetries lifts both the valley degeneracy of Landau levels and, particularly, the additional two-fold degeneracy of the lowest LL. In addition, we found the optical strengths and determined the selection rules for inter-LL transitions.

Acknowledgments

Authors would like to thank O Pankratov for discussions. This project has been funded by EPSRC-GB Portfolio Partnership EP/C511743/1 and EPSRC-GB First Grant EP/E063519/1.

References

[1] Novoselov K S, Geim A K, Morozov S V, Jiang D, Zhang Y, Dubonos S V, Grigorieva I V and Firsov A A 2004 *Science* **306** 666
[2] Katsnelson M I 2007 *Mater. Today* **10** 20
[3] Geim A K and Novoselov K S 2007 *Nat. Mater.* **6** 183
[4] Katsnelson M I and Novoselov K S 2007 *Solid State Commun.* **143** 3
[5] Castro Neto A H, Guinea F, Peres N M R, Novoselov K S and Geim A K 2009 *Rev. Mod. Phys.* **81** 109
[6] Berger C, Song Z, Li T, Li X, Ogbazghi A Y, Feng R, Dai Z, Marchenkov A N, Conrad E H, First P N and de Heer W A 2004 *J. Phys. Chem.* B **108** 19912
[7] Berger C, Song Z, Li X, Wu X, Brown N, Naud C, Mayou D, Li T, Hass J, Marchenkov A N, Conrad E H, First P N and de Heer W A 2006 *Science* **312** 1191
[8] Rollings E, Gweon G-H, Zhou S Y, Mun B S, McChesney J L, Hussain B S, Federov A V, First P N, de Heer W A and Lanzara A 2006 *J. Phys. Chem. Solids* **67** 2172
[9] Sadowski M L, Martinez G, Potemski M, Berger C and de Heer W A 2006 *Phys. Rev. Lett.* **97** 266405
[10] Sadowski M L, Martinez G, Potemski M, Berger C and de Heer W A 2007 *Solid State Commun.* **143** 123
[11] Jiang Z, Henriksen E A, Tung L C, Wang Y-J, Schwartz M E, Han M Y, Kim P and Stormer H L 2007 *Phys. Rev. Lett.* **98** 197403
[12] Deacon R S, Chuang K-C, Nicholas R J, Novoselov K S and Geim A K 2007 *Phys. Rev.* B **76** 081406(R)
[13] Plochocka P, Faugeras C, Orlita M, Sadowski M L, Martinez G, Potemski M, Goerbig M O, Fuchs J-N, Berger C and de Heer W A 2008 *Phys. Rev. Lett.* **100** 087401
[14] Henriksen E A, Jiang Z, Tung L-C, Schwartz M E, Takita M, Wang Y-J, Kim P and Stormer H L 2008 *Phys. Rev. Lett.* **100** 087403
[15] McCann E 2006 *Phys. Rev.* B **74** 161403(R)
[16] Castro E V, Novoselov K S, Morozov S V, Peres N M R, Lopes dos Santos J M B, Nilsson J, Guinea F, Geim A K and Castro Neto A H 2007 *Phys. Rev. Lett.* **99** 216802
[17] Min H, Sahn B, Banerjee S K and MacDonald A H 2007 *Phys. Rev.* B **75** 155115
[18] Stauber T, Peres N M R, Guinea F and Castro Neto A H 2007 *Phys. Rev.* B **75** 115425
[19] Pereira J M Jr, Peeters F M and Vasilopoulos P 2007 *Phys. Rev.* B **76** 115419
[20] Ohta T, Bostwick A, Seyller T, Horn K and Rotenberg E 2006 *Science* **313** 951
[21] Oostinga J B, Heersche H B, Liu X, Morpurgo A F and Vandersypen L M K 2008 *Nat. Mater.* **7** 151
[22] McCann E and Fal'ko V I 2006 *Phys. Rev. Lett.* **96** 086805
[23] McClure J W 1957 *Phys. Rev.* **108** 612
[24] Slonczewski J C and Weiss P R 1958 *Phys. Rev.* **109** 272
[25] Mucha-Kruczynski M, Tsyplyatyev O, Grishin A, McCann E, Fal'ko V I, Bostwick A and Rotenberg E 2008 *Phys. Rev.* B **77** 195403
[26] McClure J W 1960 *Phys. Rev.* **119** 606
[27] Dresselhaus G and Dresselhaus M S 1965 *Phys. Rev.* **140** A401
[28] Nakao K 1976 *J. Phys. Soc. Japan* **40** 761
[29] Abergel D S L and Fal'ko V I 2007 *Phys. Rev.* B **75** 155430
[30] Novoselov K S, McCann E, Morozov S V, Fal'ko V I, Katsnelson M I, Zeitler U, Jiang D, Schedin F and Geim A K 2006 *Nat. Phys.* **2** 177